EPR parameters of E' centers in v-SiO_2 from first-principles calculations

Luigi Giacomazzi,[1,*] L. Martin-Samos,[1,2] A. Boukenter,[3] Y. Ouerdane,[3] S. Girard,[3] and N. Richard[4]

[1]*CNR-IOM/Democritos National Simulation Center, Istituto Officina dei Materiali, c/o SISSA, via Bonomea 265, IT-34136 Trieste, Italy*

[2]*Materials Research Laboratory, University of Nova Gorica, Vipavska 11c 5270-Ajdovščina, Slovenija*

[3]*Laboratoire Hubert Curien, UMR-CNRS 5516, F42000 Saint-Etienne, France*

[4]*CEA, DAM, DIF, F-91297 Arpajon, France*

(Received 25 February 2014; revised manuscript received 3 July 2014; published 28 July 2014)

A first-principles investigation of E' centers in vitreous silica (v-SiO_2) based on calculations of the electron paramagnetic resonance (EPR) parameters is presented. The EPR parameters are obtained by exploiting the gauge including projector augmented wave method as implemented in the QUANTUM-ESPRESSO package. First, we analyze the EPR parameters of a large number of Si_2 dimers. The g tensor of the Si_2 dimers is shown to possess an average rhombic symmetry and larger g principal values with respect to those observed, e.g., for the E'_γ center in silica. Furthermore, the g principal values clearly show a linear trend with the Si-Si dimer length. Our results suggest that the Si_2 dimers could correspond to an unidentified paramagnetic center, though occasionally the calculated g principal values of the Si_2 dimer might be compatible with those found experimentally for the E'_δ center. Next, we generate nondimer configurations by a procedure involving structural relaxations in the subsequent positively charged states. In particular, puckered, unpuckered, doubly puckered, and forward-oriented configurations are generated. The distributions of the calculated EPR parameters of the puckered and unpuckered configurations further support the assignment of the E'_γ center to an unpaired spin localized at a threefold coordinated silicon dangling bond. Moreover, by analyzing Fermi contacts and g tensors of the puckered and forward-oriented configurations, we suggest the assignment of the E'_α center to the latter type of configurations. This work also suggests that the differences in the EPR parameters of E'_α and E'_γ centers mainly arise from the strained geometry of the silicon dangling bond. In the forward-oriented configurations, one Si-O bond is about 0.2 Å longer than the remaining two, whereas in the silicon dangling bond of the puckered and unpuckered configurations, all three bonds have a length of ∼1.6 Å each.

DOI: 10.1103/PhysRevB.90.014108 PACS number(s): 61.72.J−, 71.15.Mb, 71.55.Jv, 76.30.Mi

I. INTRODUCTION

The discovery of paramagnetic pointlike defects in irradiated quartz and vitreous silica (v-SiO_2) dates back to the early electron paramagnetic resonance (EPR) investigations done by Weeks in the 1950s on a particular class of defects, the E' centers [1,2]. These defects not only constitute a major class of intrinsic defects in silicon dioxide, but they also deeply affect the performances of electronic and optical devices, especially in radiation environments that lead to an increase in their concentration. For instance, E' centers are responsible for the appearance of an absorption band at 5.8 eV in the UV range [3]. Despite its long history, research on radiation-induced color centers, such as the E' centers in silica, is still of paramount importance for the production of improved materials and devices needed for applications in harsh environments such as nuclear power plants and space missions [4,5]. Furthermore, the aim of designing radiation-tolerant optical fibers for the development of facilities devoted to fusion, such as the International Thermonuclear Experimental Reactor (ITER), the Laser Megajoule (LMJ), or the National Ignition Facility (NIF) [6–8], constitutes a common effort of both the industrial and scientific communities. One of the essential conditions for the success of these projects is a better understanding of the physical properties of defects [9,10].

Despite the fact that about 15 varieties of E' centers [11] are known to exist in silica-based glasses, only a few of them pertain to the pure v-SiO_2 network. The most studied one, known as E'_γ (analogous to the E'_1 center in α quartz [12,13]), is experimentally characterized by a strong ($A_{iso} \sim 42$ mT) hyperfine splittings (hfs) on a ^{29}Si nucleus. The E'_γ is commonly attributed to a localized unpaired electron of a Si sp^3 dangling bond (DB) in a $\cdot Si \equiv O$ unit (where $\equiv$ represents bonds to three distinct O atoms, and $\cdot$ is an unpaired electron) [14–21].

Besides the E'_γ center, two other paramagnetic point defects, E'_α and E'_δ, are known in pure v-SiO_2 [22–24]. E'_α is characterized by very strong hyperfine splittings (49 mT) and by an orthorhombic g tensor. Moreover, the 49 mT doublet is characterized by a slightly larger FWHM with respect to that observed for the 42 mT doublet of the E'_γ [25]. About a decade ago, Mukhopadhyay *et al.* [26] studied the structure and properties of neutral and positively charged oxygen vacancies in v-SiO_2 by using an embedded cluster method and found out that the majority of dangling bond centers are unpuckered. Reference [26] quite remarkably predicted the existence of a back-projected dangling bond with high hyperfine splittings (48.9 mT) that was later regarded as a possible candidate to explain the origin of the E'_α center [25,27]. However, Ref. [26] did not calculate the g-tensor principal values of the investigated configurations, leaving open the possibility of other explanations of the E'_α center. More recently, g-tensor calculations of a few oxygen vacancy configurations (forward-oriented and puckered configurations) in v-SiO_2 were carried out by Uchino *et al.* [28]. Quite interestingly, in Ref. [28] the $A_{iso}(^{29}Si)$ parameter calculated for the forward-oriented configurations appears to differ by a few mT with respect to

*giacomaz@sissa.it

the Fermi contact of puckered configurations. Furthermore, g principal values of the forward-oriented configurations are strongly orthorhombic as compared to puckered and bridged hole-trapping oxygen-deficiency center (BHODC) configurations. In contrast to the most accepted models [26,29], the latter configuration type was suggested to be responsible for the E'_γ center [28]. The E'_δ center has an almost isotropic EPR resonance line ($g \sim 2.002$) together with hyperfine splittings of $\sim$10 mT [24,30]. The origin of the E'_δ center is even more controversial [31]. It is supposed to arise either from an interaction of an unpaired electron in a sp^3-like orbital delocalized over four or five nearby ^{29}Si, or from an ionized single oxygen vacancy with the unpaired electron shared nearly equally by the two neighboring Si atoms (Si_2 dimer center). Though several theoretical works [17,26,32,33] support the Si_2 dimer hypothesis, they do not explain the intensity ratio between the main EPR resonance line and the 10 mT hyperfine doublet that seems to be better explained by assuming an E' center involving at least four Si atoms [31,34]. Richard *et al.* [35] have shown that for a positively charged oxygen vacancy, the dimer configuration appears to be the lowest-energy configuration with an 80% probability, in agreement with previous theoretical investigations [29]. The results obtained by Refs. [35] and [29] contrast with the apparent absence of any EPR signal arising from positively charged Si_2 dimers [31].

By accurate first-principles calculations of the g tensors and Fermi contacts of a large number of positively charged oxygen vacancy configurations, we provide here a detailed analysis of the EPR hyperfine parameters and g-tensor principal values of Si_2 dimer, puckered, and forward-oriented configurations. The present work does not address the issues related to the existence of precursors of the E' centers prior to irradiation and focuses only on the assignment of the known E' EPR signals to specific electronic structure models. We emphasize that oxygen vacancies are employed here not as a precursor model of the E' centers, but just as a technical expedient to obtain a sufficiently large statistical set of paramagnetic centers. We take advantage of a 108-atom model of v-SiO_2 that has previously been adopted to study the optical absorption of neutral defects in silica [36]. By applying a procedure involving subsequent relaxations with different charging states, as outlined in the next section, we generate a total of 72 independent dimer configurations, as well as 47 puckered, 11 unpuckered, 5 forward-oriented, and a thermodynamically irrelevant double-puckered configurations. This large set of configurations allows us to well describe the distributions of EPR parameters of each type of configuration in terms of local structural parameters. In particular, we show that g principal values of the Si_2 dimer configurations feature a linear trend with Si-Si dimer length. EPR parameters of puckered and unpuckered configurations are discussed in terms of their Si-Si distance (i.e., the distance between the Si dangling bond carrying the unpaired electron and the silicon atom carrying the hole) [35]. Furthermore, it is shown that the distribution of Fermi contacts of puckered and unpuckered configurations displays a linear trend when crossed with the g_2 or g_3 principal values. Forward-oriented (FO) configurations show a rather different behavior because of their large g_2 values. This suggests that FO configurations could give rise to EPR signals not overlapping with those pertaining to the E'_γ center, shown here to be originated by an unpaired electron of a Si dangling bond as found, e.g., in puckered and unpuckered configurations. In particular, the average g values and Fermi contacts (and their spreads) calculated for FO configurations support an assignment of the E'_α center as mainly originating from these configurations.

The paper is organized as follows: in Sec. I, we introduce the main issues concerning the E' centers in silica; in Sec. II, we give the technical details of the theoretical methodology and modeling of the E' centers. In Sec. III, for each defect configuration type, we first describe the structure and then show the results of our calculations of g tensors and hyperfine parameters. In particular, we discuss Si_2 dimers (Sec. III A), puckered and unpuckered (Sec. III B), forward-oriented (Sec. III C), and doubly puckered (Sec. III D) configurations. We provide distributions showing how the g tensors and Fermi contacts vary with Si-Si length. Results are also discussed by considering quantities helpful for describing the examined configurations such as dangling bond angles and distances between the silicon dangling bond and atoms in two-membered rings. Section III E is dedicated to the discussion of the results and a comparison of them with available experimental data of E' centers in vitreous silica. Finally, in Sec. IV, we draw the conclusions of our work, and in the Appendix we discuss the relative stability (by considering energy differences) of the investigated configurations of positively charged oxygen vacancies.

II. THEORETICAL METHODOLOGY AND MODELING DETAILS

The calculations carried out in this work are based on density functional theory (DFT). In particular, the Perdew-Burke-Ernzerhof (PBE) exchange-correlation functional has been adopted for the present calculations [37]. Norm-conserving Trouiller-Martins pseudopotentials are used and Kohn-Sham wave functions are expanded in a basis of plane waves up to a kinetic cutoff of 80 Ry [38]. The wave functions were expanded at the sole Γ point of the Brillouin zone, as justified by the large size and the large band gap of our system [36]. Geometry optimizations and EPR parameters have been obtained by means of spin-polarized calculations, unless otherwise specified. Occupations of states are fixed to be either 1 or 0. The codes used for the present calculations are freely available with the QUANTUM-ESPRESSO (QE) package v5.0.1 [39].

The defect-free v-SiO_2 model consists of a periodic supercell containing 108 atoms and 576 electrons [35]. We generated oxygen-deficient center (ODC) configurations by considering each oxygen site in the silica model. Every ODC configuration was generated by removing a bridging oxygen and an electron from the original defect-free silica model and by subsequently relaxing the structure by using the Broyden-Fletcher-Goldfarb-Shanno (BFGS) algorithm as implemented in the pw.x code [39]. A force threshold of 0.000 75 Ryd/bohr has been adopted. Due to the presence of an energy barrier between the dimer configuration and the puckered ones, the outcome of this first relaxation is always a positively charged Si_2 dimer. In order to generate

other configurations of the positively charged oxygen vacancy (e.g., puckered), we further relaxed each Si_2 configuration in the following way. First we further charged the system by removing a second electron and then performed a relaxation. Since the relaxation in a +2 charged state is done with the sole purpose of obtaining nondimer configurations, non-spin-polarized calculations were performed. The configurations so obtained in the +2 charged state were then used as the starting point for a new relaxation in the +1 charged state. For all of the defect models in this work, the final relaxation in the +1 charged state was performed with the BFGS algorithm and with the same PBE gauge including projector augmented wave (GIPAW) pseudopotentials used later for the EPR calculations [39]. EPR hyperfine couplings and g tensors can be calculated with a good accuracy by employing DFT-based methods such as the GIPAW method. Such method enables the calculation of nuclear magnetic resonance (NMR) and EPR parameters in solids using periodic boundary conditions. In particular, for the present work, we used the QE-GIPAW code from the QE package [39] for the calculation of the EPR parameters of our set of charged oxygen vacancy models.

To ensure that the size of our silica model is sufficient to provide reasonably well-converged g principal values, we first tested the convergence versus **k**-points mesh of the g principal values of a positively charged oxygen vacancy in α quartz. Converged values are identical to those reported in Ref. [38] for the E'_1 center, where four inequivalent **k** points and a 71-atom supercell were used. By comparing between the converged g-tensor values of the E'_1 center in α quartz and of equivalent (puckered) configurations in v-SiO_2, we estimate a size error corresponding to a systematic overestimation of up to ∼150 ppm for the calculated g principal values in v-SiO_2. The aforementioned error is smaller than fluctuations caused by the structural disorder and does not affect assignments and conclusions based on the presented results.

III. RESULTS

By following the procedure outlined in Sec. II, we obtained several different types of positively charged oxygen vacancies (Table I). In this section, for each configuration type (Si_2 dimer, puckered, unpuckered, doubly puckered, and forward-oriented configurations), we give a description of the atomic structure of the defect together with an analysis of the EPR parameters (Fermi contacts and g tensors). In particular, we discuss how EPR parameters vary with local structural parameters, such as the Si-Si separation (d_{SiSi}) and dangling bond angle of the first-principles relaxed structures.

TABLE I. Configuration type, number of configurations N, average relative energy ΔE (eV), and average Si-Si distance $\langle d_{SiSi}\rangle$ between the two Si atoms originally neighboring the positively charged oxygen vacancy as after *ab initio* relaxation, together with their standard deviations (in parentheses). Relative energies are given with respect to the lowest-energy configuration.

Configuration type	Figure	N	ΔE (eV)	$\langle d_{SiSi}\rangle$
Si_2 dimer	1(a)	72	0.7(0.3)	2.94(0.24)
Puckered	1(d)–1(g)	47	1.0(0.4)	4.78(0.75)
4×	1(d)–1(f)	13	0.7(0.4)	5.07(0.66)
5×	1(f), 1(g)	34	1.1(0.3)	4.66(0.76)
Unpuckered	1(b), 1(c)	11	1.3(0.1)	4.56(0.57)
FO	1(h)	5	0.4(0.3)	3.07(0.11)
DP	1(i)	1	1.9	5.37

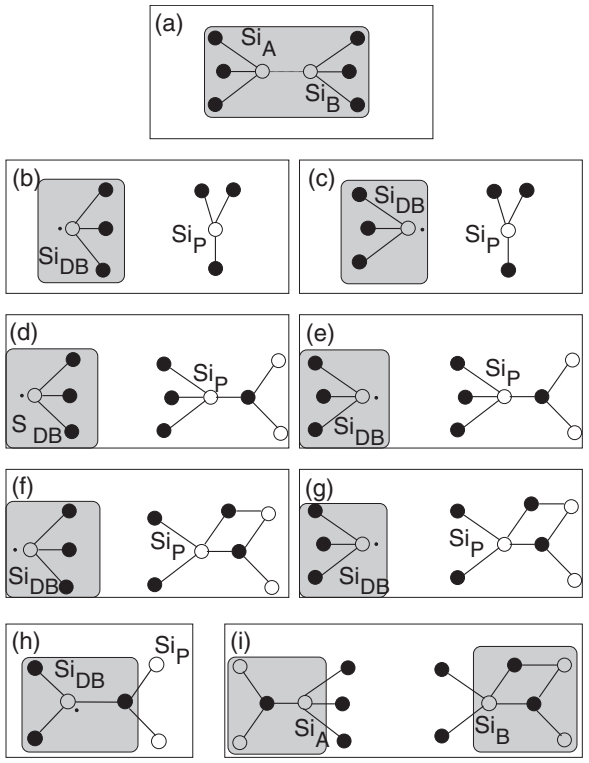

FIG. 1. Summary of the configuration types of positively charged oxygen vacancies generated by following the procedure outlined in Sec. II: (a) Si_2 dimer, (b) back-projected unpuckered, (c) forward-projected unpuckered, (d) back-projected puckered 4×, (e) forward-projected puckered 4×, (f) back-projected puckered 5×, (g) forward-projected puckered 5×, (h) forward-oriented, and (i) doubly puckered configurations. Oxygen (filled disk) and silicon (empty disk) atoms and the unpaired electron (dot) are shown. The shaded area indicates the relevant local environment of the paramagnetic center. Si-Si distances discussed in the text (d_{SiSi}) are taken between silicon atoms labeled with Si_{DB} and Si_P in (b)–(g) and between Si_A and Si_B in (a) and (h).

A. Si_2 dimers

1. *Structure*

First, a large set of Si_2 dimers [Fig. 1(a)] is found (72 configurations). We obtain Si_2 dimer configurations with Si-Si dimer lengths (d_{SiSi}) varying from ∼2.6 to ∼3.8 Å. The spin density is localized mainly in the region between the two Si atoms [Fig. 2(a)]. In the Si_2 dimers, the average Si-O bond length is 1.60 Å with a standard deviation (std) of 0.01 Å, while the average bond angle ⟨O-Si-O⟩ is 114.7° with a std of 0.7°, indicating that silicon atoms lie in an intermediate position between an ideal flat geometry (120°) and a lone-pair sp^3 geometry (∼108°).

In Table I, we also give the average Si-Si distance between the two Si atoms of the oxygen vacancy and average relative

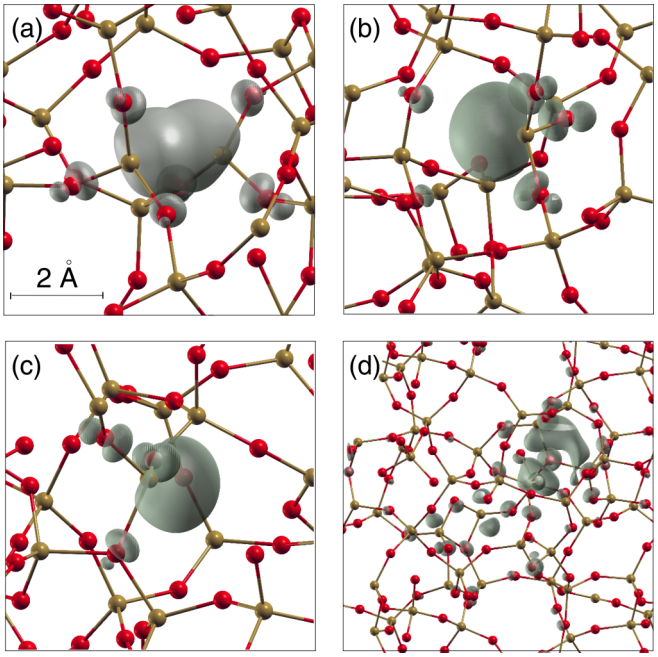

FIG. 2. (Color online) Ball and stick models and spin densities of (a) Si_2 dimer, (b) puckered, (c) forward-oriented (FO), and (d) doubly puckered (DP) configurations in v-SiO_2 [40]. Red spheres correspond to oxygen atoms, light brown spheres correspond to silicon atoms, and spin density is shown with a transparent gray color. The same axis scales are used in (a)–(c), while (d) is plotted by using a scale factor of 0.5 with respect to (a).

energy with respect to the lowest-energy configuration. Si_2 dimers have a rather long average Si-Si dimer length with respect to the one previously calculated with a local density approximation (LDA) functional (2.8 Å) [35]. The effect is partly explained by the use of a PBE functional that leads to a Si-Si elongation of ∼0.07 Å with respect to LDA calculations. On the other hand, here we considered a different and larger set of dimer configurations with respect to those of Ref. [35].

2. *Fermi contacts and g tensors*

In Fig. 3(a), we show the g-tensor principal values versus d_{SiSi} as calculated for the Si_2 dimer configurations [Fig. 1(a)]. On average, the three g principal values appear to differ by about 500 ppm and all of them show an average decrease of 180 ppm each 0.1 Å. We note a rather large variability of the g values vs Si-Si dimer length that might make Si_2 dimers rather difficult to be detected. For d_{SiSi} around 3.0 Å, the g-tensor principal values are quite close to the free electron value $g_e = 2.002\,32$. Moreover, a few of the Si_2 dimers show EPR parameters that are nearly identical to those observed for the E'_δ center, but with the cost of a rather high energy [∼1 eV larger than the lowest-energy dimers of Fig. 10(a)]. In Table II, we give the g principal values averaged over all of the investigated Si_2 dimers. These values are rather different from those typical of the E' centers in pure silica [21–24]. For large enough Si-Si lengths, the g principal values start to show some similarity with those of the E'_γ center [22] as it should be since we expect the unpaired electron to become more localized on one of the two Si atoms surrounding the oxygen vacancy.

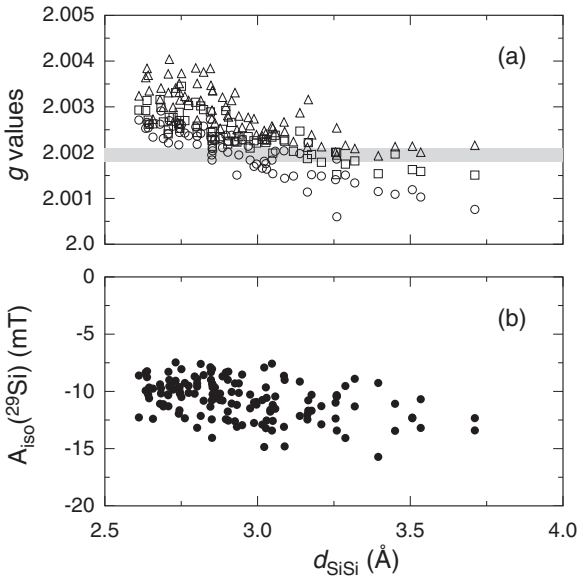

FIG. 3. Calculated (a) g-tensor principal values g_1 (circles), g_2 (squares), g_3 (triangles) and (b) Fermi contact of ^{29}Si atoms in positively charged Si_2 dimers vs Si-Si dimer length. The shaded area shows the range of experimental g values [24].

Indeed, for a $d_{SiSi} \geqslant 3.5$ Å, we register g principal values: $g_1 \sim 2.0010$, $g_2 \sim 2.0015$, and $g_3 \sim 2.0020$. Furthermore, if we consider that the lower-energy configurations are those with lower dimer Si-Si lengths, we might expect Si_2 dimers to give rise to an EPR signal with g principal values close to ∼2.003. Indeed, for $d_{SiSi} \leqslant 2.9$ Å, the average g principal values are $g_1 = 2.0023$, $g_2 = 2.0027$, and $g_3 = 2.0033$ with a standard deviation (std) of 400 ppm.

In Fig. 3(b), we show the Fermi contacts distribution of ^{29}Si atoms in our Si_2 dimers. We found a large spread of values (−8 to −16 mT) and a small decrease with increasing Si-Si dimer length, indicating a tendency of the spin density to become more localized on the dimer Si atoms.

B. Puckered and unpuckered configurations

1. *Structure: Unpuckered configuration*

Second, another type of configuration is given by well-separated (about 4.6 Å) threefold Si atoms, of which one is the Si dangling bond (Si^{DB}) while the other is a "puckered" positive Si atom (Si^{P}). This configuration cannot relax into a puckered one because the oxygens of the background are too far to allow the formation of a new Si^{P}-O bond. On the other hand, threefold silicon atoms are too separated to form a dimer as in Fig. 1(a). We refer to this type of configuration as unpuckered DB [Figs. 1(b) and 1(c)] for which we register a total of 11 structures.

For the unpuckered configuration type, the calculated average $\langle O\text{-}Si^{DB}\text{-}O\rangle$ is 107.5° with a std of 1.1° as expected for a sp^3 hybridized dangling bond orbital, while $\langle O\text{-}Si^{P}\text{-}O\rangle$ is 119.9° indicating that the Si^{P} lies in the plane of its three oxygen neighbors. The $O\text{-}Si^{DB}$ bond length is, on average, 1.65 Å, while the average $O\text{-}Si^{P}$ is much shorter, 1.57 Å. Both lengths have a std of 0.01 Å.

TABLE II. Configuration type, g principal values g_1, g_2, g_3, and Fermi contact $A_{iso}(^{29}Si)$ (mT) of Si_2 dimer, puckered, unpuckered, DP, and FO configurations together with their standard deviations (in parentheses). Energies are given with respect to the lowest-energy configuration. For comparison, experimental g principal values together with their experimental error (in parentheses) and experimental hyperfine splittings together with their FWHM (in parentheses) are given for E'_γ, E'_α, and E'_δ centers.

Configuration type	Figure	g_1	g_2	g_3	$A_{iso}(^{29}Si)$
		Theory			
Si_2 dimer	1(a)	2.002 00 (52)	2.002 41(44)	2.002 87(55)	− 10.7(1.7)
Unpuckered	1(b),1(c)	2.001 90(6)	2.000 57(19)	2.000 17(10)	− 40.3(2.1)
Puckered	1(d)–1(g)	2.001 86(9)	2.000 55(18)	2.000 17(16)	− 41.1(2.6)
4×	1(d),1(e)	2.001 84(7)	2.000 53(17)	2.000 15(14)	− 41.4(2.3)
5×	1(f),1(g)	2.001 87(10)	2.000 56(19)	2.000 18(17)	− 41.0(2.7)
DP	1(i)	2.009 95	2.009 25	2.009 25	− 5.0(1.7)
FO	1(h)	2.001 89(18)	2.001 03(15)	1.999 37(28)	− 47.8(0.8)
		Experiments			
E'_γ		2.001 75(4)[a]	2.000 56(4)[a]	2.000 30(4)[a]	42(3)[b]
E'_α		2.0018(1)[b]	2.0009(1)[b]	1.9997(1)[b]	49(4)[b]
E'_δ		2.0018(1)[c]	2.0020(1)[c]	2.0020(1)[c]	10(1.5)[d]

[a]Reference [49].
[b]Reference [25].
[c]Reference [31].
[d]Reference [50].

For the dangling bond in puckered and unpuckered configurations, a further distinction can be made between back-projected (BP) and forward-projected (FP) configurations. In the BP configurations, the threefold Si on which the unpaired electron is localized moves backward over the plane of its three oxygen neighbors, pointing away from the center of the vacancy [Figs. 1(b), 1(d), and 1(f)]. By contrast, in the FP configurations, the Si dangling bond points towards the center of the vacancy [Figs. 1(c), 1(e), and 1(g)]. Figs. 1(b)–1(g) correspond to the microscopic structures of the E'_γ center as proposed by several theoretical and experimental investigations [15,19,26,27]. A modified version of the structure shown in Fig. 1(b), where the unpaired spin is perturbed by the presence of a close background oxygen, has been regarded as a possible explanation of the E'_α center [25–27].

The unpuckered configurations are almost always back projected [Fig. 1(b)]. Only one configuration with $d_{SiSi} \sim 4.2$ Å is found forward projected as in Fig. 1(c), consistent with the fact that a FP configuration with a short d_{SiSi} could easily relax into a dimer configuration, i.e., no significant energy barrier should exist between unpuckered forward-projected and dimer configurations. Thus, in the following, we do not distinguish between FP and BP orientation for unpuckered configurations.

2. *Structure: Puckered configuration*

Next, a large number (47) of puckered configurations is found. At variance with the unpuckered DB, in the puckered configuration the Si^P atom relaxes back over the plane of its three ligand oxygens in a puckered position and forms a new bond with an oxygen of the background that becomes threefold coordinated [15,35]. Puckered configurations can be further subdivided into two subgroups, here named as 4× [Figs. 1(d) and 1(e)] and 5× [Figs. 1(f) and 1(g)] following Ref. [35]. The puckered configurations of the 5× group differ from the 4× group by the presence of a two-membered ring with a threefold oxygen atom [35].

The spin density of a puckered configuration is shown in Fig. 2(b), where the unpaired electron appears strongly localized on the lone pair of the threefold silicon atom and around its three oxygen neighbors. In puckered configurations, the calculated average silicon dangling bond angle ⟨O-Si^{DB}-O⟩ is 108.6° with std of 0.7°, consistent with the tetrahedral geometry given by sp^3 hybridization. We found a O-Si^{DB} bond length of 1.65 Å, only slightly larger than the average Si-O bond length in our v-SiO_2 models (1.63 Å). All three of the Si-O bonds formed by the threefold oxygen ($O^{[3]}$) are quite long [15]. In particular, the one formed with the puckered silicon atom (Si^P) has a bond length of 1.84 Å, while the remaining two bonds have lengths of 1.77 Å, considerably larger (8–12%) than the average length.

Puckered 4× configurations show a rather long Si-Si distance d_{SiSi} (Table I), i.e., the two Si atoms that originally surround the oxygen vacancy after the first-principles relaxation of the atomic structure become largely separated. This is because the majority of the puckered 4× configurations are back projected and have a $d_{SiSi} \geqslant 5$ Å [see Figs. 10(b) and 10(c) in the Appendix]. In contrast, the puckered 5× configurations show a rather low Si-Si distance due to the large number of FP puckered 5× configurations with $d_{SiSi} \leqslant 4.5$ Å.

3. *Fermi contacts and g tensors*

In Fig. 4, we show the calculated g principal values and Fermi contacts of puckered, unpuckered, and forward-oriented configurations (Sec. III C) obtained as described in Sec. II. Average g principal values and Fermi contacts of the investigated configurations are given in Table II.

Puckered configurations show d_{SiSi} ranging from ∼3.5 to ∼7 Å (the maximum allowed distance within the cell is 10 Å). We note that g values in the range 3.5–4.0 Å, most of which correspond to the FP puckered 5× configurations, appear to

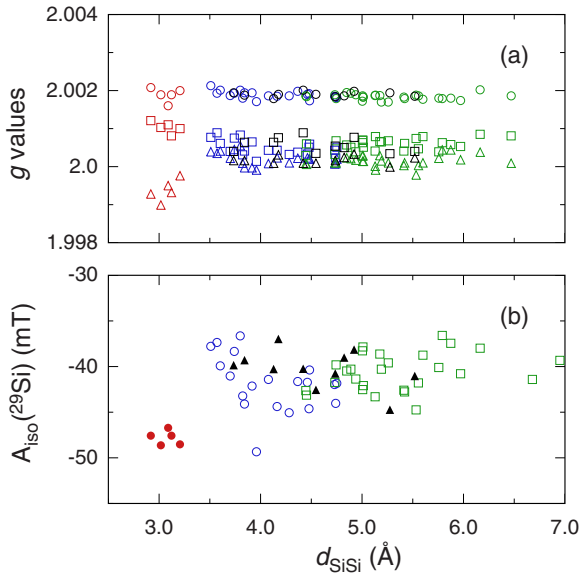

FIG. 4. (Color online) Calculated (a) g principal values: g_1 (circles), g_2 (squares), g_3 (triangles), and (b) Fermi contacts of FO (red discs), back-projected puckered (green squares), forward-projected puckered (blue circles), and unpuckered (black triangles) configurations vs Si-Si distance.

show large fluctuations resembling a decreasing trend with increasing d_{SiSi}. For $d_{\mathrm{SiSi}} \geqslant 4.0$ Å, the calculated g values do not show any particular dependence on d_{SiSi}.

The average Fermi contact of all puckered and unpuckered configurations is -41.0 mT with a std of 2.5 mT [41]. Dangling bonds in amorphous silicon are known to show a linear relation between the Fermi contact and the mean bond angle between the DB atom and its back-bonded neighbors [42]. In Fig. 5, we show the calculated Fermi contact of all Si DB configurations plotted vs the DB bond angle. We consider all of our puckered and unpuckered configurations [43]. At variance with amorphous silicon [42], here no linear trend is found and the data is rather scattered, suggesting that the local environment of the $\mathrm{Si^{DB}}$ heavily affects the spin density and thus the $A_{\mathrm{iso}}(^{29}\mathrm{Si})$ value.

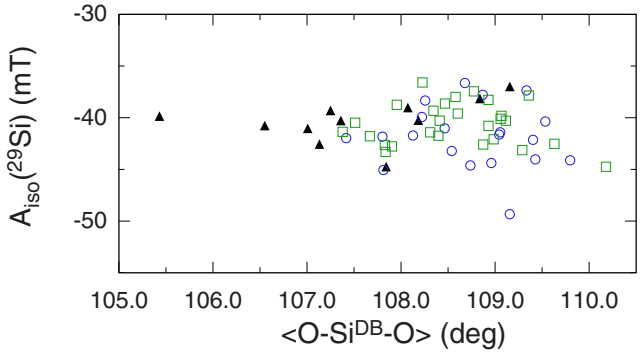

FIG. 5. (Color online) Fermi contacts of back-projected (green squares), forward-projected (blue circles), and puckered and unpuckered (black triangles) configurations plotted vs average dangling bond angle $\langle \mathrm{O\text{-}Si^{DB}\text{-}O} \rangle$.

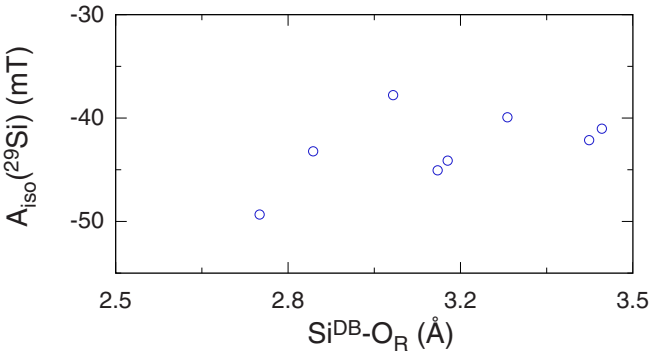

FIG. 6. (Color online) Fermi contacts of forward-projected puckered 5× configurations plotted vs $\mathrm{Si^{DB}\text{-}O_R}$ distance, where $\mathrm{O_R}$ is the nearest oxygen of the two-membered ring.

The $A_{\mathrm{iso}}(^{29}\mathrm{Si})$ Fermi contact of the FP puckered 5× configurations could correlate with the distance of the Si dangling bond from the two-membered ring taken as distance $\mathrm{Si\text{-}O_R}$, where $\mathrm{O_R}$ is the nearest oxygen of the two-membered ring, as might be suggested by Fig. 6. Data beyond ∼3.5 Å do not show any particular correlation with $\mathrm{Si\text{-}O_R}$ distance and thus are not included in Fig. 6. Moreover, the few data points in Fig. 6 are still rather scattered as a consequence of different local environment and of different orientation of the $\mathrm{Si^{DB}}$ with respect to the two-membered ring.

C. Forward-oriented configurations

1. Structure

Among the generated oxygen vacancies, we found five configurations of the forward-oriented (FO) type [28]. The FO configuration type [Fig. 1(h)] is similar to the geometry of the transition state of the interconversion path between ODCs found by Donadio *et al.* [44]. In the forward-oriented configurations, a $\mathrm{Si^{DB}}$ and a threefold oxygen ($\mathrm{O^{[3]}}$) become nearest neighbors. The average bond length between the $\mathrm{Si^{DB}}$ and the threefold oxygen is 1.83 Å with a std of 0.03 Å, considerably longer then the other two remaining $\mathrm{O\text{-}Si^{DB}}$ bonds which have identical lengths of 1.62 Å with a std of 0.01 Å. The spin density resembles the one given by the unpaired electron in the puckered and unpuckered configurations [Figs. 2(c) and 2(b)]. Consistently with their geometry [Fig. 1(h)], FO configurations have $d_{\mathrm{SiSi}} \sim 3.1$ Å, i.e., the Si-Si nearest-neighbors distance in v-$\mathrm{SiO_2}$. The average dangling bond $\langle \mathrm{O\text{-}Si^{DB}\text{-}O} \rangle$ angle is 108.0° with a std of 0.6°, very similar to unpuckered and puckered configurations. The average $\langle \mathrm{Si\text{-}O^{[3]}\text{-}Si} \rangle$ angle in FO configurations is ∼119.1° with a std of 7.8°, but in the highest-energy FO configuration [Fig. 10(a) in the Appendix], we found a lower angle (118.8°) with a much larger spread (17.4°), indicating a markedly strained configuration.

2. Fermi contacts and g tensors

The g values in Fig. 4(a) corresponding to short Si-Si distances ($d_{\mathrm{SiSi}} \leqslant 3.2$ Å) between the two Si atoms originally surrounding the oxygen vacancies belong to the forward-oriented configurations [28]. These are rather low-energy

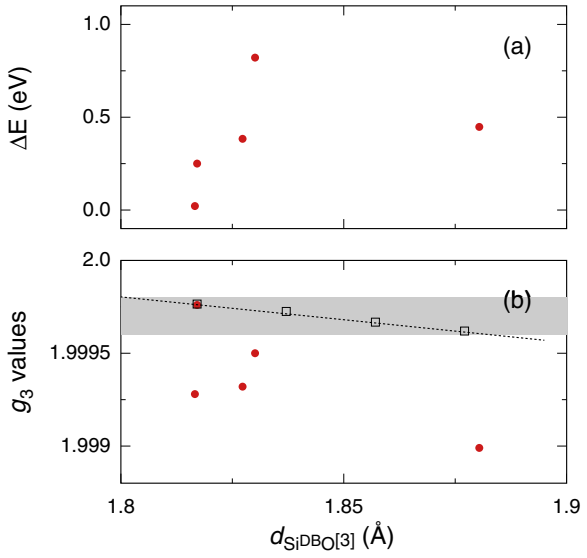

FIG. 7. (Color online) Calculated (a) relative energy and (b) g_3 principal values plotted vs bond length ($d_{Si^{DB}O[3]}$) between the threefold silicon and the threefold oxygen atom in forward-oriented (FO) configurations [Fig. 1(g)]. Shaded area shows the experimental range of g_3 values of the E'_α [25]. The dotted line and empty symbols show the decreasing of g_3 vs $d_{Si^{DB}O[3]}$ calculated as explained in the text.

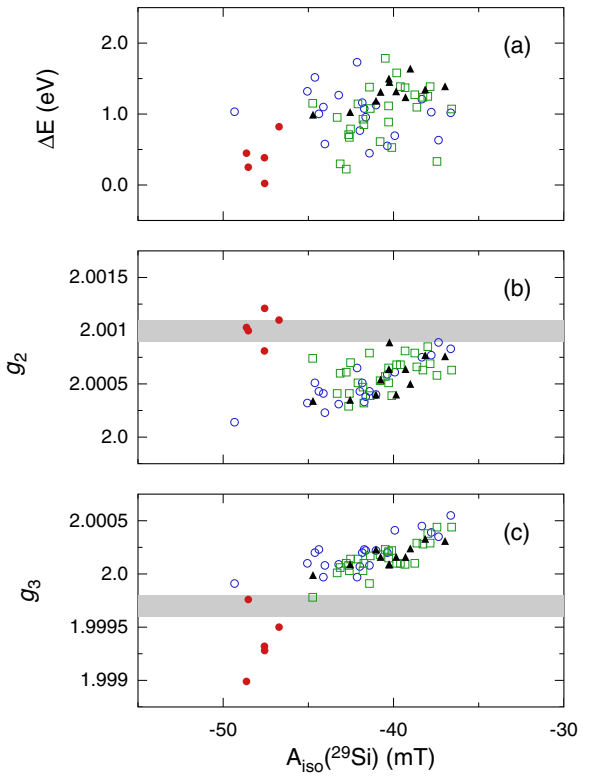

FIG. 8. (Color online) (a) Relative energy, (b) g_2, and (c) g_3 principal values of forward-projected (blue circles) and back-projected (green squares), puckered, unpuckered (black filled triangles), and FO (red discs) configurations plotted versus the corresponding Fermi contacts. Shaded area shows the experimental range of g_2 and g_3 values of the E'_α [25].

configurations [see Fig. 10(b) in the Appendix] with respect to those typical of the puckered or unpuckered configurations. Figure 4(a) suggests that g values pertaining to the forward-oriented configurations should not correspond to the same paramagnetic defect given by puckered or unpuckered configurations. The average g values of FO configuration are $g_1 = 2.001\,89(18)$, $g_2 = 2.001\,03(15)$, and $g_3 = 1.999\,37(28)$. The rather large spread found for the g_3 value (0.000 28) might signal the existence of a correlation with some structural parameter, as, for example, the dependence on Si-Si distance of the g values of the Si_2 dimer configurations that explains the large spreads of the first row of Table II. We note that the relative energies of the FO configurations seem to increase with increasing bond length ($d_{Si^{DB}O[3]}$) between the threefold silicon and the threefold oxygen atom [Fig. 7(a)]. Moreover, the rather high-energy configuration with $d_{Si^{DB}O[3]} \sim 1.88$ Å shows low g_3 values ($\sim$1.9990), while the three configurations at $d_{Si^{DB}O[3]} \leqslant 1.82$ Å correspond to the following average g values: $g_1 \sim 2.001\,99(10)$, $g_2 \sim 2.001\,01(20)$, $g_3 \sim 1.999\,45(27)$ [Fig. 7(b)]. We explicitly checked the effect of an increase of $d_{Si^{DB}O[3]}$ first by displacing the threefold oxygen by 0.02, 0.04, and 0.06 Å along the direction $O^{[3]}$-Si^{DB} for the FO configuration shown at $g_3 = 1.999\,76$ in Fig. 7(b). Next we performed a structural relaxation of the atomic positions, except for the $O^{[3]}$ and Si^{DB} atoms, and finally we calculated the g-tensor principal values as explained in Sec. II. The g_3 so calculated shows a linear decrease with a slope of -2.5×10^{-3} Å^{-1} as shown in Fig. 7(b) [45].

The spreads of the FO g values reported in Table II are similar to those found for the puckered and unpuckered distributions. We note also that g_2, g_3 differ by at least three std with respect to the g_2, g_3 found for the puckered and unpuckered configurations, further suggesting that the FO configurations give rise to a distinguishable EPR signal not overlapping with the one corresponding to the puckered configurations. FO configurations show a larger (in magnitude) Fermi contact (−47.8 mT) with a rather smaller std (0.8 mT) as compared to puckered configurations. The small value of the spread of the Fermi contacts is likely to be biased by the small number (five) of FO configurations considered here and is expected to increase for larger statistical samples of FO configurations.

In Fig. 8(a), we plot the relative energy of puckered, unpuckered, and forward-oriented configurations versus their Fermi contact values. Below $\sim$−45 mT, forward-oriented configurations show the lowest energies, while unpuckered, forward-projected, and back-projected puckered configurations have larger energies by $\sim$0.5 eV [46]. In Figs. 8(b) and 8(c), we plot the g_2 and g_3 principal values of puckered, unpuckered, and forward-oriented configurations against their Fermi contacts (g_1 is not shown since for all of the configurations, we found rather constant values at $\sim$2.0019). The g_2 values of the puckered and unpuckered configurations are broadly distributed around a kind of increasing linear trend with increasing Fermi contacts. We note that we found configurations at $g_2 \sim 2.0010$ for Fermi contacts at $\sim$−48 mT (FO configurations) or larger than $\sim$−40 mT (puckered and unpuckered). Similarly, in Fig. 8(c), we show the existence

of an increasing trend of g_3 versus Fermi contact for the puckered and unpuckered configurations going from 1.9998 at −49 mT up to 2.0006 at −37 mT. The g_3 values of forward-oriented configurations do not display any particular trend with Fermi contacts, though they are more vertically spread (from 1.9990 to 1.9997) with respect to the g_2 values of the FO configurations in Fig. 8(b).

D. Doubly puckered configuration

The last type of configuration analyzed in this work is a doubly puckered (DP) configuration [Fig. 1(i)] of which we have only a single configuration. At variance with puckered configurations, here both of the silicon atoms are back projected over the plane of the oxygen neighbors and form a new bond with an oxygen of the background that becomes threefold coordinated. Consequently, the DP configuration has a $d_{\mathrm{SiSi}} \sim 5.4$ Å comparable to those registered for the BP puckered 4× and 5× configurations. We note that the spin density is not localized in a Si dangling bond, as in puckered configurations, but appears mainly delocalized over the silicon neighbors of threefold coordinated oxygen atoms [Fig. 2(d)]. Both of the threefold oxygen atoms show rather long Si-O bond lengths (1.76–1.86 Å) as previously seen for the threefold oxygen in puckered configurations.

The DP configuration is very different from all of the other E' related defects. The unpaired electron occupies a defect state just below (∼1 eV) the bottom of the conduction band. This type of defect thus corresponds to a thermodynamically unstable state and could be stabilized only if the Fermi level was kept as high as almost the whole silica band gap, a condition which is unlikely to occur even in an extremely harsh environment.

The DP configuration has a rather high relative energy (Table I) and gives rise to a quite isotropic g tensor not belonging to the usual list of E' centers. As the spin density of this paramagnetic defect is delocalized over several (at least four) Si atoms, this multicenter defect has a rather small Fermi contact, $A_{\mathrm{iso}}(^{29}\mathrm{Si}) \approx -5$ mT, and its g principal values are around 2.009, which, as far as we know, does not correspond to any observed EPR signal in pure v-SiO_2.

E. Discussion

1. Si *DB configurations originating the* E'_γ

The puckered and unpuckered configurations show similar average g principal values, Fermi contacts, and energies. Consequently, both types of configurations should be regarded as sources of the E'_γ center in v-SiO_2. As shown in Table II, we register, for these configurations, an exceptionally good agreement with the experimental EPR data available for the E'_γ so that it seems quite unlikely that other explanations may exist for this defect, in contrast to the conclusions of Uchino *et al.* [28]. It should also be noted that our analysis of a large number of silicon dangling bond configurations shows that only a minor fraction of them is of the (back-projected) unpuckered type, whereas this was previously claimed to constitute the majority of dangling bond centers [26]. Moreover, among the puckered (FP, BP, 4×, 5×) and unpuckered configurations considered herein, we do not see any particular group of configurations that could correspond to any other kind of EPR signal, except for the E'_γ center. A way to distinguish between such types of configurations could be, e.g., by analyzing irradiated silica samples both with EPR and Raman spectroscopies. Indeed, localized vibrational modes of two-membered rings, such as those in puckered 5× configurations, are likely to explain the origin of a feature at 900 cm^{-1} in the Raman spectrum of irradiated silica, as recently seen by Leon *et al.* [47].

We do not *a priori* exclude the possibility that other configurations may contribute to the E'_γ center besides the puckered and unpuckered configurations as, e.g., the BHODC configuration [28]. However, with the adopted procedure for generating positively charged oxygen vacancies, we did not find any BHODC configuration. The latter is more likely related to the E'_γ center, although by inspecting Table I of Ref. [28], one cannot exclude that the BHODC, if present, may also contribute to the broadening of the hyperfine splittings doublet of the E'_α.

2. E'_α *vs forward-oriented configurations*

By inspecting a short list of the experimentally detected paramagnetic defects in v-SiO_2 (Table II) and also by taking into account the calculated g principal values of Table II, we infer that E'_α should be associated with forward-oriented configurations [48]. These might not be the only ones related to the E'_α center. Indeed, Ref. [26] has shown that back-projected puckered configurations can give rise to strong hyperfine couplings if the silicon carrying the unpaired spin "interacts" with a nearby background oxygen [25,26]. Among our back-projected puckered configurations, we could find one with a rather large Fermi contact (−45 mT) and g tensor ($g_2 = 2.000\,74$ and $g_3 = 1.9998$) resembling the E'_α one [Figs. 8(b) and 8(c)]. Though the spin density of this configuration is mostly localized at the silicon dangling bond, as in the usual E'_γ picture, we note that a nearby oxygen [at a distance of 3.05 Å from the silicon dangling bond in a front position; see Fig. 9(a)] also shows spin localization. The close proximity of this background oxygen (O^B) results in a more

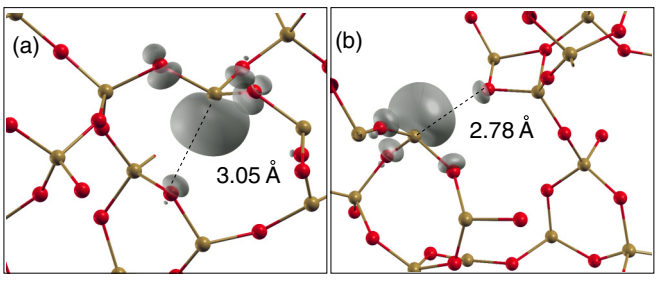

FIG. 9. (Color online) Ball and stick models and spin densities of (a) a back-projected configuration in which the silicon dangling bond points towards a background oxygen placed at 3.05 Å distance, and (b) a forward-projected configuration in which the silicon dangling bond points towards an oxygen atom belonging to a twofold ring and placed at 2.78 Å from the silicon atom. This spin density in (a) corresponds to the −45 mT point (square) of Fig. 8, while the spin density in (b) corresponds to the −49 mT point (disc) of Fig. 8.

orthorhombic g tensor and a larger Fermi contact value [25,26]. However, given the small number of configurations showing a distance $d_{Si^{DB}O^{B}}$ of less than ∼3.2 Å between the silicon dangling bond and a background oxygen in a front position as in Fig. 9(a), we cannot study in detail how the g tensor of a back-projected configuration can vary with such a distance O^{B}-Si^{DB}. We remark that by comparing with Fig. 6, for $d_{Si^{DB}O^{B}}$ distances beyond ∼3.2 Å, the ^{29}Si Fermi contact should not be affected by the presence of a O^{B}. Furthermore, we note that when considering as precursor of the E'_{α} only the oxygen vacancy type, the relative energy of a configuration like the one in Fig. 9(a) is rather large (by ∼1 eV), indicating a lower stability as compared to the lowest puckered and forward-oriented configurations [Fig. 8(a)]. Moreover, we also found one forward-projected puckered 5× configuration with a large relative energy (∼1 eV) and a very large Fermi contact (−49 mT) as shown in Fig. 8(a). In this configuration, the threefold silicon atom carrying the unpaired spin is quite close (2.78 Å) to one oxygen of the two-membered ring formed by the puckered silicon [Fig. 9(b)]. The latter oxygen atom shows spin localization that results in a more orthorhombic g tensor and a larger Fermi contact value [25,26]. We note that due to the trend shown in Figs. 8(b) and 8(c) followed by the large majority of Si DB configurations, it seems rather unlikely that a puckered or unpuckered configuration will show the right symmetry of the g tensor of E'_{α}. Indeed, for forward-projected puckered configurations (most of which have d_{SiSi} in the range 3.5–4.0 Å), the aforementioned trend implies that for $|A_{iso}| \sim 49$ mT, $g_2 \sim 2.0001$ is evidently too low with respect to the $g_2 \sim 2.0010$ observed in the experiments for the E'_{α} center. For puckered BP configurations, one can find $g_2 \sim 2.0010$, but at the same time this implies a rather small Fermi contact ($|A_{iso}| \leqslant 42$ mT). Again this does not exclude the possibility to find a puckered BP configuration with a g tensor and Fermi contact in agreement with those observed for the E'_{α}, but, from Figs. 8(a)–8(c), this would be just the consequence of a "tail behavior" of the wide puckered configuration distribution giving rise to the E'_{γ}.

3. E'_{δ} *vs* Si_2 *dimers*

Despite the fact that the average Fermi contact calculated for ^{29}Si atoms in the Si_2 dimers is rather close to the one reported for the E'_{δ}, the dimer g-tensor symmetry does not, in general, correspond to the E'_{δ} one. The average g-tensor principal values obtained by taking into account all of the data of Fig. 3(a) are $g_1 = 2.0020$, $g_2 = 2.0024$, and $g_3 = 2.0029$, all with a std of ∼500 ppm. Moreover, if we restrict the average to the lowest-energy configurations, i.e., $d_{SiSi} \leqslant 2.9$ Å, the g principal values will be ∼400 ppm larger: $g_1 = 2.0023$, $g_2 = 2.0027$, and $g_3 = 2.0033$, with a std of 400 ppm. The former average g values are compatible with the results of previous investigations where a hybrid functional (Becke three-parameter Lee-Yang-Parr) and localized basis sets were used but only a few dimer configurations were analyzed [28,32]. It is also worth noting that simply averaging g values over the investigated configurations, as done in Table II, does not properly convey the most relevant information of Fig. 3(a), i.e., the strong variation of the dimer g-tensor principal values with the Si-Si dimer distance.

Thus, the calculated g-tensor symmetry of positively charged Si_2 dimers does not fulfill the isotropic symmetry shown by the E'_{δ} g tensor, and also average g_2 and g_3 values overestimate the experimental values. However, this does not prevent the fact that for a dimer length d_{SiSi} around 3 Å, it may happen that some dimers have EPR parameters similar to those known from the experiments for the E'_{δ}. Yet this would be a rather minor effect and dimer contribution to E'_{δ} would be rather difficult to detect.

IV. CONCLUSIONS

In this paper, we performed a first-principles analysis of the EPR parameters of a large statistical set of positively charged oxygen vacancies. The analysis concerned not only distributions of Fermi contacts, but also the more computationally demanding g principal values distributions. The EPR parameters of Si_2 dimers, puckered and unpuckered Si dangling bond configurations, and forward-oriented and doubly-puckered configurations were discussed here in terms of structural parameters describing the local environment of the defect.

The present analysis of positively charged Si_2 dimers does not allow for an assignment of the E'_{δ} to such a defect type or for a rejection of this hypothesis. The variation of g principal values with Si-Si may result in both the Fermi contact and g tensor falling close to the experimental EPR parameters of the E'_{δ}. On the other hand, our analysis of the g principal values distribution of Si_2 dimers indicates that Si_2 dimers should possess a g tensor with an average rhombic symmetry, in contrast to the almost isotropic g tensor obtained from the EPR experiments for the E'_{δ} center. In any case, new investigations are required to clearly establish whether or not a relation exists between Si_2 dimers and the E'_{δ} center.

The calculations further confirm that the E'_{γ} center should be attributed to an unpaired electron in a sp^3 state at a threefold coordinated silicon atom, in agreement with previous theoretical and experimental investigations. In particular, in this paper, we demonstrated that the distributions of both puckered and unpuckered Si dangling bond configurations give rise to the same paramagnetic defect. Furthermore, the unpuckered configurations show a larger average relative energy with respect to puckered 5× and 4× configurations. Using this energy criterion, our work suggests that among the E'_{γ}-like configurations, the puckered 4× one is the most stable variant under thermodynamic equilibrium. Yet, under irradiation, the relative concentration of charged defects becomes a nonequilibrium dynamical quantity, the estimation of which is far beyond the scope of the present paper. Moreover, it is shown that the local environment can strongly affect the EPR parameters of the Si dangling bond by considerably varying the Fermi contact (up to 15%) and the g_2 and g_3 principal values (up to ∼500 ppm) with respect to their average values.

The comparison of the Fermi contacts and g principal value distributions calculated for puckered and forward-oriented configurations suggests that the dominant paramagnetic defect giving rise to the E'_{α} is not a puckered (or an unpuckered) Si

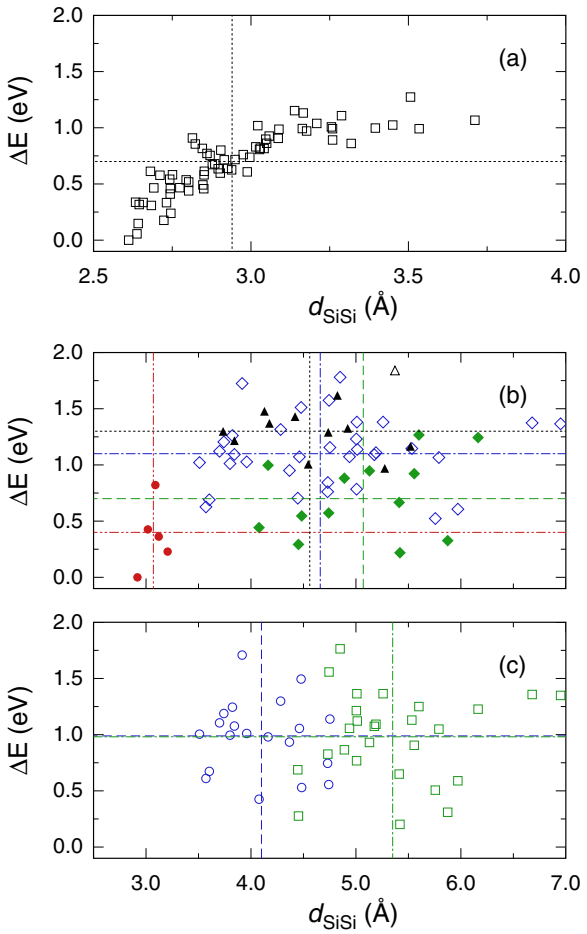

FIG. 10. (Color online) Relative energy (ΔE) with respect to the lowest-energy dimer configuration. (a) Relative energy (ΔE) with respect to the lowest-energy configuration of positively charged Si_2 dimers vs Si-Si dimer length (d_{SiSi}). (b) Puckered 4× (green filled rhombs), 5× (blue rhombs), forward-oriented FO (red discs), unpuckered (black filled triangles), and doubly puckered DP (triangle) configurations. (c) Relative energy of forward-projected (blue circles) and back-projected (green squares) puckered configurations. For each configuration type, vertical and horizontal lines are used, respectively, to indicate the average d_{SiSi} and the average relative energy.

dangling bond configuration, but rather is the forward-oriented configuration, where a threefold coordinated oxygen and a threefold coordinated silicon carrying the unpaired spin are nearest neighbors.

Besides the above-mentioned configurations, here we discussed the EPR parameters of a doubly puckered configuration. Being localized just below the conduction band, this is an unstable defect with a clear non-E' character and, as far as we know, does not correspond to any observed EPR signal in pure v-SiO_2. Finally, the present work has shown the reliability of the first-principles approach for calculating the EPR parameters for some of the main defects known to have an effect on the transmission of silica-based glasses.

ACKNOWLEDGMENTS

We acknowledge A. Alessi and T. E. Jones for their careful reading of the manuscript and the helpful comments. We also acknowledge M. Cannas, S. De Gironcoli, M. Farnesi Camellone, and D. Ceresoli for their useful comments and suggestions. The calculations in this work were performed using the HPC resources of CINECA (Project No. EPRFIBER-HP10B4CVBH) and of GENCI-CCRT (Grant No. 2013096137).

APPENDIX: RELATIVE ENERGIES

In Fig. 10(a), we give the relative energy of the Si_2 dimers vs d_{SiSi}, illustrating the relative stability of our dimer configurations. A trend is discernible so that the shorter the Si-Si dimer length is, the lower is the energy of the configuration. Since the formation energy should show a similar trend as the one in Fig. 10(a), this implies that the most frequent dimers in v-SiO_2 should be those with a short Si-Si length. In particular, it seems quite unlikely to find Si_2 dimers with $d_{SiSi} \sim 3$ Å, i.e., having ∼1 eV higher formation energies than Si_2 dimers with $d_{SiSi} \sim 2.6$ Å.

In Fig. 10(b), we show the relative energies of puckered, unpuckered, FO, and doubly puckered configurations to illustrate their relative stability with respect to our lowest-energy configuration (a dimer). FO configurations have rather low relative energies, suggesting a high stability as found for Si_2 dimers. Puckered 4× configurations have slightly larger relative energies, though comparable to the average energy of dimers, as shown in Table I (0.7 eV). The relative energy of puckered 5× configurations is larger with respect to puckered 4× by 0.4 eV, as a consequence of the presence of the two-membered ring, and in fair agreement with the difference (0.57 eV) in formation energies reported in Ref. [35]. Unpuckered configurations have an even larger relative energy, indicating a rather low stability of this kind of defect (that probably should easily relax into another configuration type). Moreover, in Fig. 10(b), the thermodynamically unstable doubly puckered configuration is shown to have the largest relative energy (1.9 eV). In Fig. 10(c), we show the relative stability of FP and BP puckered configurations. Both types show a similar spread of values so that FP or BP orientation allows for a similar stability range. Quite interestingly we note that only FP configurations occur for $d_{SiSi} \leqslant 4.5$ Å, while BP configurations dominate for $d_{SiSi} \geqslant 5$ Å.

By comparing the relative energies of each oxygen vacancy site between the Si_2 dimer configuration and the corresponding nondimer configuration (FO, puckered, unpuckered, DP), we found that for the large majority of the vacancy sites, the Si_2 dimer configuration has the lowest energy (73.6%). The puckered and FO configurations result in the lowest-energy configuration for 20.8% and 5.6% of the analyzed oxygen vacancy sites, while unpuckered configurations are never the minimum-energy configuration. These findings are in agreement with the LDA results of Ref. [35], but for the occurrence of the FO configurations that have a large relative stability as compared to the other configuration types. This suggests that the FO configurations are likely to have formation energies as low as (or even lower than) the Si_2 dimers and puckered DB configurations.

[1] R. A. Weeks, J. Appl. Phys. **27**, 1376 (1956).
[2] R. A. Weeks and C. M. Nelson, J. Am. Ceram. Soc. **43**, 399 (1960).
[3] L. Skuja, J. Non-Cryst. Solids **239**, 16 (1998).
[4] S. J. Mihailov, Sensors **12**, 1898 (2012).
[5] J. R. Schwank, M. R. Shaneyfelt, D. M. Fleetwood, J. A. Felix, P. E. Dodd, P. Paillet, and V. Ferlet-Cavrois, IEEE Trans. Nucl. Sci. **55**, 1833 (2008); H. L. Hughes and J. M. Benedetto, *ibid.* **50**, 500 (2003).
[6] W. J. Hogan *et al.*, Nucl. Fusion **41**, 567 (2001).
[7] T. Kakuta *et al.*, J. Nucl. Mater. **307**, 1277 (2002).
[8] S. Girard *et al.*, IEEE Trans. Nucl. Sci. **52**, 1497 (2005).
[9] J. L. Bourgade *et al.*, Rev. Sci. Instrum. **79**, 10F304 (2008).
[10] S. Girard *et al.*, IEEE Trans. Nucl. Sci. **60**, 2015 (2013).
[11] R. A. Weeks, R. H. Magruder III, and A. Stesman, J. Non-Cryst. Solids **354**, 208 (2008).
[12] M. Boero, A. Oshiyama, and P. L. Silvestrelli, Phys. Rev. Lett. **91**, 206401 (2003).
[13] M. Boero, A. Oshiyama, and P. L. Silvestrelli, Mod. Phys. Lett. B **18**, 707 (2004).
[14] J. K. Rudra and W. B. Fowler, Phys. Rev. B **35**, 8223 (1987).
[15] M. Boero, A. Pasquarello, J. Sarnthein, and R. Car, Phys. Rev. Lett. **78**, 887 (1997).
[16] A. Stirling and A. Pasquarello, Phys. Rev. B **66**, 245201 (2002).
[17] P. E. Blöchl, Phys. Rev. B **62**, 6158 (2000).
[18] S. Agnello, R. Boscaino, G. Buscarino, M. Cannas, and F. M. Gelardi, Phys. Rev. B **66**, 113201 (2002).
[19] M. Cook and D. L. Griscom, J. Non-Cryst. Solids **182**, 119 (1995).
[20] G. Pacchioni and M. Vitiello, Phys. Rev. B **58**, 7745 (1998).
[21] D. L. Griscom, Phys. Rev. B **20**, 1823 (1979).
[22] D. L. Griscom, in *Defects in SiO_2 and Related Dielectrics: Science and Technology*, edited by G. Pacchioni, L. Skuja, and D. L. Griscom, (Kluwer Academic, Dordrecht, 2000), p. 117.
[23] D. L. Griscom, Nucl. Inst. Methods B **1**, 481 (1984).
[24] D. L. Griscom and E. J. Friebele, Phys. Rev. B **34**, 7524 (1986).
[25] G. Buscarino, S. Agnello, and F. M. Gelardi, Phys. Rev. Lett. **97**, 135502 (2006).
[26] S. Mukhopadhyay, P. V. Sushko, A. M. Stoneham, and A. L. Shluger, Phys. Rev. B **70**, 195203 (2004).
[27] G. Buscarino, R. Boscaino, S. Agnello, and F. M. Gelardi, Phys. Rev. B **77**, 155214 (2008).
[28] T. Uchino and T. Yoko, Phys. Rev. B **74**, 125203 (2006).
[29] Z. Y. Lu, C. J. Nicklaw, D. M. Fleetwood, R. D. Schrimpf, and S. T. Pantelides, Phys. Rev. Lett. **89**, 285505 (2002).
[30] G. Buscarino, S. Agnello, and F. M. Gelardi, Phys. Rev. B **73**, 045208 (2006).
[31] M. Jivanescu, A. Stesmans, and V. V. Afanas'ev, Phys. Rev. B **83**, 094118 (2011).
[32] S. Mukhopadhyay, P. V. Sushko, A. M. Stoneham, and A. L. Shluger, J. Phys.: Condens. Matter **17**, 1311 (2005).
[33] B. R. Tuttle and S. T. Pantelides, Phys. Rev. B **79**, 115206 (2009).
[34] G. Buscarino, S. Agnello, and F. M. Gelardi, Phys. Rev. Lett. **94**, 125501 (2005).
[35] N. Richard, L. Martin-Samos, G. Roma, Y. Limoge, and J.-P. Crocombette, J. Non-Cryst. Solids **351**, 1825 (2005).
[36] N. Richard, L. Martin-Samos, S. Girard, A. Ruini, A. Boukenter, Y. Ouerdane, and J-P. Meunier, J. Phys.: Condens. Matter **25**, 335502 (2013).
[37] J. P. Perdew, K. Burke, and M. Ernzerhof, Phys. Rev. Lett. **77**, 3865 (1996).
[38] C. J. Pickard and F. Mauri, Phys. Rev. Lett. **88**, 086403 (2002).
[39] P. Giannozzi *et al.*, J. Phys.: Condens. Matter **21**, 395502 (2009); http://www.quantum-espresso.org
[40] Spin-density plots have been carried out by using XCRYSDEN (http://www.xcrysden.org/). Isosurfaces are plotted for a density value corresponding to 0.1 of the maximum value.
[41] We note that the std of Fermi contact in puckered and unpuckered configurations is very close to the FWHM as found in the experiments for the E'_γ center [21,25]. This suggests that the FWHM is mainly caused by variations of the local environment of the ^{29}Si dangling bond.
[42] G. Pfanner, C. Freysoldt, J. Neugebauer, and U. Gerstmann, Phys. Rev. B **85**, 195202 (2012).
[43] The DB bond angles of the forward-oriented configurations are not considered because of their different geometry of the silicon dangling bond. Indeed, in the FO configurations, one O-SI^{DB} bond is remarkably longer than the other two, resulting in a rather perturbed FO spin density and Fermi contact with respect to those of the puckered and unpuckered configurations.
[44] D. Donadio, M. Bernasconi, and M. Boero, Phys. Rev. Lett. **87**, 195504 (2001).
[45] By varying $d_{\mathrm{Si^{DB}O^{[3]}}}$, the calculated g_2 principal value displays a smaller variation with respect to g_3 (with a slope of $\sim 1.0 \times 10^{-3}$ Å^{-1}), while g_1 shows only a negligible variation with respect to the one calculated for g_3.
[46] Back-projected configurations with distances of $\sim$2.6 Å between the silicon dangling bond site and the background oxygen were also found, in Ref. [26], to show larger energies with respect to other dangling bond configurations.
[47] M. Leon, L. Giacomazzi, S. Girard, N. Richard, P. Martin, L. Martin-Samos, A. Ibarra, A. Boukenter, and Y. Ouerdane, IEEE Trans. Nucl. Sci. (2014), doi:10.1109/TNS.2013.2294033.
[48] The absolute values of the hyperfine parameters given in Table II could slightly change by considering core-polarization effects and relativistic corrections [42,51–53]. By contrast, the relative difference between the average Fermi contacts of puckered and FO configurations is expected to be independent of the adopted approximations. The results of Table II indicate that the Fermi contact of the puckered and FO configurations should differ by about 7 mT. Since the experimental 42 mT hfs signal is attributed to the unpaired spin of a ^{29}Si DB as, e.g., it is found here in puckered and unpuckered configurations, our calculations show that the FO configurations should originate an EPR signal featuring hfs of $\sim$49 mT.
[49] A. Stesmans, K. Clémer, and V. V. Afanas'ev, Phys. Rev. B **72**, 155335 (2005).
[50] A. Stesmans, M. Jivanescu, and V. V. Afanas'ev, Europhys. Lett. **93**, 16002 (2011).
[51] J. R. Yates and C. J. Pickard, *Computations of Magnetic Resonance Parameters for Crystalline Systems: Principles* (Wiley, Chichester, UK, 2008).
[52] M. S. Bahramy, M. H. F. Sluiter, and Y. Kawazoe, Phys. Rev. B **76**, 035124 (2007).

[53] Hyperfine parameters in Table II are given without core-polarization corrections [52,54], which can be calculated with an experimental feature available with QE v5.0.1. We found that such corrections account for ∼10% of the absolute value of Fermi contacts of puckered, unpuckered, and FO configurations, while in dimers the corrections account for ∼15%.

[54] V. Filidou, D. Ceresoli, J. J. L. Morton, and F. Giustino, Phys. Rev. B **85**, 115430 (2012).